A classical path theory of collisional redistribution in CaHe spinchanging energy transfer collisions

S. Ananthamurthy, K. M. Sando, and P. D. Kleiber

Citation: The Journal of Chemical Physics **101**, 10485 (1994); doi: 10.1063/1.467867
View online: http://dx.doi.org/10.1063/1.467867
View Table of Contents: http://scitation.aip.org/content/aip/journal/jcp/101/12?ver=pdfcov
Published by the AIP Publishing

A classical path theory of collisional redistribution in CaHe spin-changing energy transfer collisions

S. Ananthamurthy
Department of Physics and Astronomy, University of Iowa, Iowa City, Iowa 52242

K. M. Sando
Department of Chemistry, University of Iowa, Iowa City, Iowa 52242

P. D. Kleiber
Department of Physics and Astronomy, University of Iowa, Iowa City, Iowa 52242

(Received 5 April 1994; accepted 15 September 1994)

We have applied a semiclassical (classical path quantum close-coupling) nonadiabatic theory of collisional redistribution to model Ca–He spin-changing energy transfer collisions. The theory predicts the total far wing absorption and final state resolved action spectra. The semiclassical model predictions are in excellent agreement with full quantum mechanical close-coupling calculations [J. Chem. Phys. **95**, 5861 (1991)] and both are in good accord with the experimental observations. © *1994 American Institute of Physics.*

I. INTRODUCTION

The spin-changing process,

$$\mathrm{Ca}^*(5p\ ^1P)+\mathrm{He}\rightarrow+\mathrm{Ca}^*(5p\ ^3P)+\mathrm{He}+\Delta E, \qquad (1)$$

has served as a benchmark for both experimental and theoretical study of nonadiabatic effects in collisional energy transfer.[1–11] Leone and co-workers have studied this process in both gas phase kinetics experiments[1] and in a series of crossed atomic beam experiments using laser polarized (orbitally aligned) metal atoms.[2–4] They measured the spin-changing cross section to be quite large (~25 Å^2), and determined that the reaction is substantially more likely when the Ca*($5p\ ^1P$) orbital is aligned initially perpendicular to the collision axis than if aligned parallel.[1–4]

In the orbital locking and following model,[12,13] the excited Ca*($5p\ ^1P$) orbital is assumed to lock onto the Ca–He internuclear axis and to follow this axis adiabatically through the collision. The perpendicular alignment should lead predominantly to excitation of the $5p\ ^1\Pi$ state of the CaHe molecule, while parallel alignment can be identified with $5p\ ^1\Sigma^+$ state excitation. In this context the experimentally observed polarization or alignment effect indicates that the reaction occurs preferentially through the $^1\Pi$ state of the complex. It is important to note, however, that the adiabatic orbital following model is not strictly valid. In essence, it amounts to neglecting the effect of nonadiabatic $^1\Pi-{}^1\Sigma^+$ rotational mixing in the entrance channel. Therefore, the magnitude of the observed experimental polarization effect reflects not only an average over velocity spread and impact parameters but also the mitigating effect of rotational coupling early in the collision encounter.

Based on these observations, Leone and co-workers have proposed that the energy transfer is facilitated by spin–orbit coupling at a short-range curve crossing between the attractive CaHe($5p\ ^1\Pi$) molecular state which correlates with the Ca*($5p\ ^1P$) level, and a repulsive CaHe($5p\ ^3\Sigma^+$) state which correlates with the lower lying atomic Ca*($5p\ ^3P$) asymptote[1–4] (Fig. 1).

These experiments have been quantitatively modeled by Alexander and Pouilly in a quantum close-coupling calculation using adjustable model potential energy curves,[7] and in a multichannel quantum defect calculation by Dubs *et al.*[8] These theoretical results support the mechanism proposed by Leone *et al.*[1–4]

An alternative experimental approach to the study of orbital alignment effects on collision dynamics involves the use of far-wing laser absorption techniques.[9,10,14] In the far or quasistatic wing of a collision-broadened atomic spectral line, the Franck–Condon approximation describes an absorption event as occurring at a fixed internuclear separation between well-defined adiabatic Born–Oppenheimer states of the transient collision complex. This makes it possible to selectively excite states of well-characterized electronic symmetry, corresponding to states of specific reagent electronic orbital alignment in the collision complex. The total absorption profiles in such experiments are determined largely by the shape of the intermolecular potential energy curves. Final state resolved measurements of the far-wing action spectra are sensitive to the dynamical evolution through the excited state "half-collision" from the Condon point of excitation into the asymptotic distribution of product states, giving insight into the nonadiabatic couplings in the exit channel. We have applied these techniques to a study of CaHe collisional energy transfer.[9,10]

In these experiments, a laser was tuned into the collision-broadened wings of the Ca($4s^2\ ^1S-5p\ ^1P$) transition, directly exciting the CaHe "quasimolecule."[9,10] This excited, unstable CaHe molecule either evolves through the collision into the Ca*($5p\ ^1P$) level or "predissociates" via the spin–orbit curve crossing to the Ca*($5p\ ^3P$) manifold (Fig. 1). The process may be represented as

$$\mathrm{Ca}(4s^2\ ^1S)+\mathrm{He}+h\nu_L\rightarrow[\mathrm{CaHe}(4s^2\ ^1\Sigma^+)]+h\nu_L \rightarrow[\mathrm{CaHe}(5p\,^1\Pi\ \text{or}\ ^1\Sigma^+)]^*, \qquad (2)$$

followed by

 0021-9606/94/101(12)/10485/8/$6.00

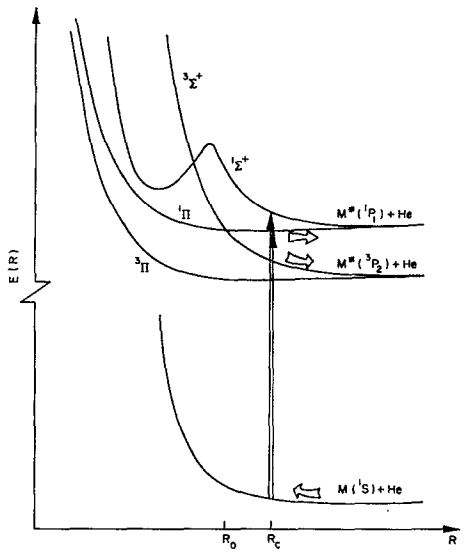

FIG. 1. Model adiabatic Born–Oppenheimer potential energy curves for the Ca–He energy transfer system. Excitation occurs near the Condon point R_c. The energy transfer process is facilitated by a spin–orbit curve crossing at R_0.

$$[\mathrm{CaHe}(5p\ ^1\Pi \text{ or } ^1\Sigma^+)]^* \rightarrow \mathrm{Ca}^*(5p\ ^1P) + \mathrm{He} \qquad (2')$$

or

$$\rightarrow \mathrm{Ca}^*(5p\ ^3P) + \mathrm{He}. \qquad (2'')$$

Based on model potential energy curves, we qualitatively expect that absorption in the far red wing should predominantly excite the attractive CaHe($5p\ ^1\Pi$) state, while blue wing absorption probably corresponds to excitation of the repulsive CaHe($5p\ ^1\Sigma^+$) curve. Thus, these far-wing laser absorption techniques may be used to carry out orbitally aligned studies of the collision dynamics under gas cell conditions. Specifically, we have measured both the total far-wing absorption and the triplet/singlet branching profile as a function of laser detuning in the wings of the Ca($4s^2\ ^1S_0 \rightarrow 5p\ ^1P_1$) resonance transition.[9,10] We have observed a pronounced red wing/blue wing asymmetry in the branching profile[9,10] which strongly supports the conclusions originally drawn by Leone's research group[1–4] that the energy transfer results from a spin–orbit curve crossing between the attractive $5p\ ^1\Pi$ and the repulsive $5p\ ^3\Sigma^+$ states of the CaHe molecule.

Theoretical modeling of these final state resolved laser scattering experiments requires a nonadiabatic theory of collisional line broadening.[15–19] A theoretical framework has been developed by Julienne and Mies,[15–17] and applied to collisional redistribution experiments in both Sr rare-gas quasielastic collisions,[18] and Na rare-gas fine structure changing collisions.[19] In the CaHe case this modeling has been carried out by Pouilly using quantum close-coupling methods.[11] Excellent agreement with the experimental line profiles was obtained. However, in this time independent close-coupling approach, it is sometimes difficult to gain appreciable physical insight into the molecular dynamics. In addition, the complexity of the calculation makes it cumbersome to apply these techniques to more complicated multichannel and multidimensional problems.

For these reasons it is instructive to consider semiclassical methods, which may both allow more physical insight into the underlying dynamics, and which, ultimately, may be more readily applied to atom-molecule chemically reactive systems. One such approach is a time dependent classical trajectory (or quasiclassical) close-coupling method.[20–23] This semiclassical approach is a generalization of the techniques developed by Nikitin[20] and Masnou-Seeuws and McCarroll,[21] extended to include radiative excitation during a collision through a dressed-molecule approach developed by Yakovlenko,[24] Kroll and Watson,[25] George,[26] and others.[27–29] The method has been applied by Light and Szöke[27] to the study of collisional redistribution in quasielastic scattering of Sr–Ar. Recently, Bieniek *et al.* have presented a thorough comparison of the results from a full quantum close-coupling calculation, a semiclassical (classical path) calculation, and an "orbital locking and following" treatment, for collisional redistribution in Sr rare-gas quasielastic collisions.[29] They find excellent agreement between these approaches.

Here we apply a similar semiclassical treatment to the more complex CaHe energy transfer system including important nonadiabatic spin–orbit and rotational coupling effects in the inelastic collision, and allowing for more realistic trajectories. In this semiclassical model the nuclear motion is described by a classical path on a single (average) adiabatic Born–Oppenheimer (ABO) potential energy curve. The electronic degrees of freedom, including nonadiabatic rotational and spin–orbit couplings, are treated quantum mechanically by close-coupling methods (but now in a reduced space consisting only of electronic states). The far-wing laser excitation of the quasimolecule during the collision may be treated as a curve-crossing problem, i.e., the absorption occurs primarily in the neighborhood of the Condon point R_c, a radiative crossing between rotating frame molecular states. The notion of a well-defined nuclear trajectory is of course, not rigorous; nevertheless, such semiclassical methods often give results in excellent agreement with exact quantum dynamics calculations.[23,29] The classical path method is expected to work well when the energy of relative motion is much larger than the energy differences for different channels. This ensures that the classical nuclear trajectories for distinct channels are similar.

The application of the classical path theory to the CaHe energy transfer problem allows a detailed quantitative comparison between the results of experiment,[9,10] an "exact" quantum mechanical treatment,[11] and a semiclassical calculation. The semiclassical treatment here reproduces the experimentally observed final state branching profiles,[9,10] and gives results which are in complete quantitative agreement with the more rigorous quantum close-coupling approach.[11] This validates the classical path method for calculating nonadiabatic line shapes in this system (even with He as the collision partner). In a future publication we will apply this method to model experiments in the more complex SrHe system,[30] where many more product channels are accessible

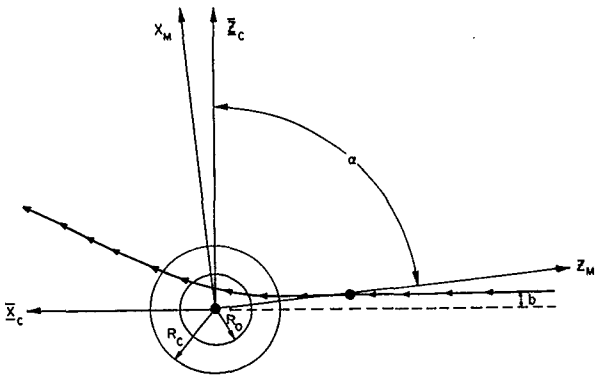

FIG. 2. Scattering process for CaHe collisions. Collision occurs with impact parameter b in the X_cZ_c plane. z_m lies along the instantaneous internuclear axis. Excitation occurs near one of two Condon points located at R_c. A Landau–Zener curve crossing occurs at R_0.

and quantum close-coupling calculations have not been attempted.

II. SEMICLASSICAL THEORY

To facilitate the discussion of the semiclassical method, we introduce three distinct coordinate systems (with coincident origins). The space-fixed laboratory frame (X_L,Y_L,Z_L) is defined by the laser polarization direction and the excitation/detection geometry. We define another space-fixed reference frame, the collision frame (X_c,Y_c,Z_c), such that the collision trajectory lies in the X_cZ_c plane with the initial velocity vector along the X_c axis. The laboratory and collision frames are related by a rotation through Euler angles (ξ,χ,ζ). Finally, we define a body-fixed molecular frame (x_m,y_m,z_m) such that y_m lies along Y_c, and z_m lies along the instantaneous internuclear axis. The molecular and collision frames are related by a time dependent rotation through angle α about the Y_c axis (Fig. 2).

The Hamiltonian for the system consisting of an atom-perturber quasimolecule in an applied electromagnetic radiation field can be expressed

$$H=H_{\rm mol}+H'_{\rm mr}, \tag{3}$$

where $H_{\rm mol}$ is the total molecular Hamiltonian, and $H'_{\rm mr}$ is the molecule-radiation dipole interaction term given by

$$H'_{\rm mr}=-e\mathbf{r}\cdot\mathbf{E}_0\cos\omega_L t. \tag{4}$$

Here $\mathbf{E}_0$ is the (slowly varying) amplitude of the applied radiation field of frequency ω_L and $e\mathbf{r}$ is the electric dipole moment operator.

$H_{\rm mol}$ can be expressed as

$$H_{\rm mol}=H_e+H', \tag{5}$$

where H_e represents the electronic Hamiltonian due to electrostatic interactions including exchange contributions. It may be written more explicitly as

$$H_e=H_{\rm Ca}+H_{\rm He}+V_{\rm coll}[R(t)], \tag{6}$$

where $H_{\rm Ca}$ and $H_{\rm He}$ describe the isolated atoms and $V_{\rm coll}$ gives the collisional interaction energy which is a function of the time-dependent internuclear separation $R(t)$. $R(t)$ describes the classical nuclear path.

The ABO potentials are the eigenvalues of the electronic structure Hamiltonian for fixed R. The adiabatic eigenstates can often be conveniently expanded in a set of Hund's case (a) basis functions $|\gamma;\Lambda S\Sigma\rangle$, where γ describes the electronic configuration, Λ is the *signed* projection of the total electronic orbital angular momentum L on the internuclear axis (sometimes called M_L), and S is the total spin with projection Σ on the molecular axis. H_e is diagonal in this basis for fixed R.

In Eq. (5), the term H' represents the most important corrections to the ABO Hamiltonian, in this case

$$H'=H'_{\rm s.o.}+H'_{\rm rot}. \tag{7}$$

$H'_{\rm s.o.}$ is the spin–orbit interaction, which we assume to be accurately approximated by the isolated Ca atomic spin–orbit operator of the form,

$$H'_{\rm s.o.}=\Sigma_i a_i\mathbf{S}_i\cdot\mathbf{L}_i, \tag{8}$$

where $\mathbf{S}_i$ and $\mathbf{L}_i$ refer to the individual electron spin and orbital angular momentum operators and the sum is over the Ca valence electrons; a_i is the atomic spin–orbit coupling parameter. $H'_{\rm rot}$ describes the rotational coupling and arises from the transformation from a space-fixed to a molecule-fixed reference frame:[22]

$$H'_{\rm rot}=-\dot{\alpha}j_y, \tag{9}$$

where $\mathbf{j}=\mathbf{L}+\mathbf{S}$ is the total electronic angular momentum. Now the Hamiltonian H is a function of time through its dependence on $R(t)$. We, therefore, solve the time-dependent Schrödinger equation,

$$i\hbar\frac{\partial\psi(t)}{\partial t}=H[R(t)]\psi(t). \tag{10}$$

The electronic wave function $\psi(t)$ can be expanded in a complete basis set of electronic eigenstates, $|n\rangle$,

$$\psi(t)=\sum_n C_n(t)|n\rangle. \tag{11}$$

Excitation in the far line wing of an atomic transition often occurs in the short-range region of internuclear distance, where the electrostatic terms dominate the Hamiltonian and H' is a small perturbation. In this limit the Hund's case (a) basis is most appropriate. $H'_{\rm rot}$ and $H'_{\rm s.o.}$ are primarily off diagonal in this basis (the diagonal contributions can be easily included in determining the ABO states), and lead to nonadiabatic coupling during the subsequent excited state evolution, between case (a) states of different Λ,S,Σ with selection rules on $\Omega(\Omega=\Lambda+\Sigma)$:$\Delta\Omega=\pm1$ for rotational coupling, and $\Delta\Omega=0$ for spin–orbit coupling.[31] As the molecule separates to sufficiently long range (where the spin–orbit interaction dominates over the electrostatic terms), a Hund's case (c) basis described by eigenstates $|n\rangle=|\gamma LSj\Omega\rangle$ is more convenient. In this basis the dominant spin–orbit terms are diagonal but the ABO difference potentials and the rota-

tional coupling terms are off-diagonal and lead to nonadiabatic coupling between the different case (c) eigenstates. Of course these bases are related through a unitary Clebsch–Gordan transformation and the dynamics may be correctly treated in either coupling scheme; the basis choice is a matter of computational convenience and personal preference. The Hund's case (i.e., the angular momentum coupling) changes as a function of R and, hence, t through the collision. It is precisely this change in coupling which leads to mixing of the ABO electronic states.[20,21] In this work we have chosen to carry out the dynamical calculations in the Hund's case (a) basis.

We may then integrate the time-dependent Schrödinger equation in this basis,

$$i\hbar \frac{dC_k(t)}{dt} = \sum_n H_{kn}(t) C_n(t) \tag{12}$$

for the eigenstate amplitudes $C_k(t)$. The Hamiltonian is a function of $R(t)$, which in turn is determined by the nuclear trajectory subject to the dynamical equations

$$\frac{dR}{dt} = v, \quad \frac{dv}{dt} = \left[-\frac{1}{\mu}\left(\frac{dV}{dR}\right)\right], \quad \frac{d\alpha}{dt} = \frac{\hbar J}{\mu R^2}, \tag{13}$$

where μ is the reduced mass and J is the total angular momentum. Here V is some average potential chosen to determine the nuclear trajectory. In practice, if the results are particularly sensitive to the choice of potential, this approach will not be tenable. For a given initial state i, the cross section $\sigma(i,f)$ for the full process including radiative excitation and nonadiabatic collisional mixing can be determined from the final asymptotic state amplitudes $a_f(+\infty)$. The initial and final states must be carefully defined to achieve convergence since radiative coupling will be important at all internuclear distances. This entails a transformation to a "dressed-molecule" frame where the full molecule+laser field Hamiltonian is diagonal.[27,28] The full Hamiltonian matrix and calculational details are discussed more completely in Sec. III. The solutions to the coupled equations (12), give the eigenstate amplitudes as a function of time, or equivalently internuclear separation, through the collision. This level of detail can give very useful physical insight into the molecular dynamics.

III. THE HAMILTONIAN

There are 12 molecular states which correlate with the excited Ca*($5p\ ^1P_1$) and Ca*($5p\ ^3P_j$) limits; including the Ca($4s^2\ ^1S_0$) ground state effectively yields a 13-state system. However, many of these states are degenerate and there are only eight distinct case (a) adiabatic Born–Oppenheimer energy levels.

The collision begins at long range with well-separated atoms in the Hund's case (c) limit. As $R\rightarrow\infty$ the collisional interaction and the rotational terms vanish (as $1/R^6$ and $1/R^2$, respectively). Thus

$$H(R\rightarrow\infty) = H_{\mathrm{Ca}} + H_{\mathrm{He}} + H'_{\mathrm{s.o.}} + H'_{\mathrm{mr}}. \tag{14}$$

In the asymptotic case (c) basis the atomic structure Hamiltonian $H_{\mathrm{Ca}} + H_{\mathrm{He}} + H'_{\mathrm{s.o.}}$ has elements given by

$$\begin{aligned} &H_{\mathrm{Ca}} + H_{\mathrm{He}} + H'_{\mathrm{s.o.}} \\ &= |L,S,j,\Omega\rangle E(L,S)\langle L,S,j,\Omega| + |L,S,j,\Omega\rangle\left(\frac{a_3}{2}\right) \\ &\quad\times[j(j+1) - L(L+1) - S(S+1)]\langle L,S,j,\Omega| \\ &\quad + |L,S=1,j=1,\Omega\rangle(a_{13})\langle L,S=0,j=1,\Omega| + \mathrm{c.c.} \end{aligned} \tag{15}$$

Here $E(L,S)$ are the isolated atomic energies (neglecting spin-orbit effects), with the Ca–He ground state chosen such that $E(L=0,S=0)=0$. The spin–orbit parameters, $a_3=9$ cm^{-1} and $a_{13}=41.8$ cm^{-1}, are assumed independent of R and are described for this system by Alexander and Pouilly.[7]

The atomic structure Hamiltonian $H_{\mathrm{Ca}} + H_{\mathrm{He}} + H'_{\mathrm{s.o.}}$ can be diagonalized by a unitary transformation $A^\dagger$, to the physical atomic eigenstates. The transformation described by Alexander and Pouilly is given by[7]

$$\begin{aligned} A^\dagger = &|L=1,S=0,j,\Omega\rangle(\cos\theta)\langle L=1,S=0,j,\Omega| \\ &+ |L=1,S=1,j,\Omega\rangle(\cos\theta)\langle L=1,S=1,j,\Omega| \\ &+ |L=1,S=0,j,\Omega\rangle(\sin\theta)\langle L=1,S=1,j,\Omega| \\ &+ |L=1,S=1,j,\Omega\rangle(-\sin\theta)\langle L=1,S=0,j,\Omega|, \end{aligned} \tag{16}$$

where θ is defined by

$$\theta = \frac{1}{2}\tan^{-1}\left(\frac{2a_{13}}{E(^1P_1) - E(^3P_1)}\right) \tag{17}$$

with a_{13} being the asymptotic off-diagonal spin–orbit coupling parameter and $E(^1P_1) - E(^3P_1)$ being the asymptotic energy level difference of the $^1P_1$ and $^3P_1$ states without the off-diagonal spin–orbit coupling.

The dipole allowed radiative transition occurs from the ground electronic state correlating with Ca($4s^2\ ^1S$), $|L=0,S=0,j=0,\Omega=0\rangle$ to the excited states correlating with Ca($5p\ ^1P$), $|L=1,S=0,j=1,\Omega\rangle$. The dipole matrix elements are of the form

$$\langle\psi_f|e\mathbf{r}\cdot\mathbf{E}|\psi_i\rangle = \langle 1,0,1,\Omega|e\mathbf{r}\cdot\mathbf{E}|0,0,0,0\rangle. \tag{18}$$

The dipole operator can be expressed in irreducible tensor form in the molecule-fixed reference frame as

$$\begin{aligned} e\mathbf{r}\cdot\mathbf{E} = &\sum_{\lambda\lambda'} d^{(1)}_{\lambda'\lambda}(\alpha) D^{*(1)}_{0\lambda}(\xi,\chi,\zeta) r^{(1)}_\lambda \frac{E_0}{2} \\ &\times[\exp(i\omega_L t) + \exp(-i\omega_L t)]. \end{aligned} \tag{19}$$

Thus,

$$\begin{aligned} \langle\psi_f|e\mathbf{r}\cdot\mathbf{E}|\psi_i\rangle = &eE_0/2\sqrt{3}[\exp(i\omega_L t) + \exp(-i\omega_L t)] \\ &\times\langle 1\|r^{(1)}\|0\rangle\left(\sum_{\lambda\lambda'} d^{(1)}_{\lambda'\lambda}(\alpha) D^{*(1)}_{0\lambda}(\xi,\chi,\zeta)\right). \end{aligned} \tag{20}$$

In essence, the rotation matrices give the projection of the laser polarization vector onto the instantaneous transition dipole moment axis.

The operator depends on the relative alignment of the laser polarization vector with respect to the molecular axis. In principle, the dynamical calculation must be carried out for a fixed collision geometry (ξ,χ,ζ), and the results averaged over all possible geometries. This will be vital if final state alignment information is sought. However, if one is not specifically interested in final state alignment effects and if the radiation field is a weak perturbation on the collision, then it is often reasonable to use an angle-averaged dipole matrix element to simplify the calculation.[16,32] Thus the electronic radiative coupling Hamiltonian matrix elements may be written as

$$H'_{\rm mr}=|1,0,j=1,\Omega\rangle\left(\frac{\bar{S}_{fi}}{2}\right)[\exp(i\omega_L t) + \exp(-i\omega_L t)]\langle 0,0,0,0|, \tag{21}$$

where $\bar{S}_{fi}$ is an effective angle-averaged Rabi frequency; $\bar{S}_{fi}\propto eE_0\langle 1\|r^{(1)}\|0\rangle$. This approximation has been justified in the weak field perturbation theory limit by Julienne and Mies,[18] and used by Pouilly.[11] A more detailed treatment of the angular problem has been given by Kovalenko *et al.* in a semiclassical calculation of alignment effects in Na–He collisions,[23] and for the case of Sr rare-gas collisional redistribution by Bieniek *et al.*[29] Ultimately the validity of such an approximation will be verified by agreement with experiment as we will see later.

We now make the unitary transformation to a rotating frame (rotating at the laser frequency, ω_L) with the transformation matrix:

$$U_R=\Sigma|L,S,j,\Omega\rangle\langle L,S,j,\Omega|+|0000\rangle[\exp(-i\omega_L t)-1] \times\langle 0000|. \tag{22}$$

The usual rotating wave approximation consists of dropping the rapidly varying terms $\propto\exp(\pm 2i\omega_L t)$.[27,28] With the rotating wave approximation the electronic radiative coupling Hamiltonian in the rotating frame becomes,

$$H'_{mR}=|1,0,j=1,\Omega\rangle\left(\frac{\bar{S}_{fi}}{2}\right)\langle 0,0,0,0|+\text{c.c.} + |0,0,0,0\rangle[E(0,0)+\hbar\omega_L]\langle 0,0,0,0|. \tag{23}$$

None of the other elements of the Hamiltonian are affected by this transformation. The effect of the rotating frame transformation is to add the energy of one laser photon $(\hbar\omega_L)$ to the ground state, so that it crosses the excited Ca*$(5p\ ^1P_1)$ manifold of states. The crossing points are exactly the Franck–Condon points of excitation (R_c). Thus the far wing laser excitation can be treated as a potential curve-crossing problem with the off-diagonal radiative coupling element given by $\bar{S}_{fi}/2$. As in the quantum close-coupling solution, this approach includes the effects of radiative absorption and nonadiabatic collisional mixing all on an equal footing.

As our dynamical calculations are carried out in Hund's case (a) this asymptotic case (c) Hamiltonian must be transformed to the case (a) basis through a standard Clebsch–Gordon transformation (C).

As the collision proceeds, the internuclear separation R decreases and the collisional and rotational interactions become important. These interactions are most conveniently described in the case (a) basis where the ABO potential energy terms are diagonal.

We first consider some of the qualitative features of the potential energy curves. We expect the long-range form of the $5p\ ^1\Sigma^+$ potential to be predominantly repulsive due to the overlap of the electron orbitals along the internuclear axis. This repulsive curve, however, shows a local maximum due to an avoided crossing with the higher-lying Ca–He$(4s6s\ ^1\Sigma^+)$ state. Conversely, the Ca–He ground state is expected to be essentially flat at long range. This qualitative picture predicts a Ca–He$(4s^2\ ^1\Sigma^+\rightarrow 4s5p\ ^1\Sigma^+)$ difference potential with a blue wing maximum leading to a classical blue wing satellite. On the other hand, the $5p\ ^1\Pi$ curve should be attractive due to the electrostatic attraction between the He atom and the Ca ionic core. This attractive $5p\ ^1\Pi$ curve crosses the lower-lying repulsive $5p\ ^3\Sigma^+$ curves that correlate to the lower-lying ^3P manifold (Fig. 1).

For these calculations we have chosen to use the potential energy curves postulated by Pouilly.[11] The Morse–Spline van der Waals' functions (MSV) used in her calculations were constructed so as to reproduce the experimentally determined quantities, such as the cross-section measurements by Leone's group[1–4] and our measurements of the branching ratios and absorption line profiles.[9,10] A detailed description of the MSV potential functions may be found in Ref. 11. Essentially the short-range behavior is described by a Morse potential, the long range by a van der Waals C_6/R^6 potential, and these limiting forms are smoothly connected with a Spline function. The MSV potentials are shown in Fig. 1.

The rotational coupling Hamiltonian is given by Eq. (9), where j_y may be written in terms of the angular momentum raising and lowering operators. Thus,

$$j_y=L_y+S_y=\frac{1}{2i}[(L_+-L_-)+(S_+-S_-)]. \tag{24}$$

The selection rules governing rotational coupling in a case (a) basis are, $\Delta\Lambda=\pm 1$ or $\Delta\Sigma=\mp 1$, and $\Delta\Omega=\pm 1$,[31] and the rotational coupling elements are evaluated from the operator relations

$$L_\pm|\Lambda,\Sigma\rangle=\sqrt{(L\mp\Lambda)(L\pm\Lambda+1)}|\Lambda\pm 1,\Sigma\rangle,$$
$$S_\pm|\Lambda,\Sigma\rangle=\sqrt{(S\mp\Sigma)(S\pm\Sigma+1)}|\Lambda,\Sigma\pm 1\rangle. \tag{25}$$

We may then numerically integrate the time dependent Schrödinger equation (12) in this basis, coupled with the dynamical equations (13) using a Runge–Kutta routine to obtain the final state amplitudes and, hence, the S matrix for the collision.

For most of our calculations we have used a simple average potential to define the classical path,

$$\bar{V}=\tfrac{1}{13}\,\mathrm{Tr}(H). \tag{26}$$

A discussion of the effect of changing this potential will be given later.

It is important to choose the initial conditions carefully since the radiative coupling terms continue to drive the popu-

lation between the ground and excited atomic states at all R.[11] For numerical convergence we must fully diagonalize the case (a) Hamiltonian at long range, i.e., transform to a set of dressed-molecule eigenstates. A rigorous discussion of this problem has been given in Mies *et al.*[33] Here we simply outline the approach for completeness. This transformation can be formally represented as $D^\dagger A^\dagger C^\dagger$, where $C^\dagger$ transforms from case (a) to (c), $A^\dagger$ diagonalizes the spin-orbit interaction, and $D^\dagger$ diagonalizes the radiative coupling (i.e., dresses the molecule). This diagonalization is actually carried out numerically at large R ($R=300a_0$ in our calculations). Although these dressed-atom eigenstates better characterize the system at large R in the presence of the laser field, the Schrödinger equation integration is carried out in a Hund's case (a) basis, and therefore the initial conditions for the integration are also specified in this basis. The physical initial condition corresponds to a bare Ca atom in its ground state. We assume that the field "turns on" slowly so that the physical atomic ground state adiabatically correlates with the dressed-atom ground state. This dressed-atom ground state may be mapped onto the Hund's case (a) basis set by the inverse transformation CAD. In other words, the case (a) amplitudes in the initial conditions are specified such that the transformation will yield a unit population (in a normalized set of states) in the physical ground state of the system. In fact, because we are in the perturbation theory limit with regard to the radiative coupling, the total absorption is always negligibly small, and it is a good approximation to assume this initial amplitude is constant. Following integration out to the asymptotic region, we map the final molecular case (a) states back onto the dressed-atom basis set (through $D^\dagger A^\dagger C^\dagger$). Then again, we assume that the laser field ultimately turns off "slowly" such that the dressed states adiabatically correlate to specific well-defined bare-atom eigenstates. In order that the field variations do not change the bare-atom eigenstates, we require that the time-dependent laser field amplitude vary slowly compared to the collision duration. The final atomic state populations are then obtained from the squares of the final state amplitudes.

IV. RESULTS AND DISCUSSION

For comparison with Pouilly's results[11] we choose the same collision energy $E=724$ cm^{-1} and radiative coupling strength $\bar{S}_{fi}/2=0.58\times10^{-2}$ cm^{-1}, which corresponds to a laser power of 1×10^5 W/cm^2, consistent with the experimental value.[9,10]

Careful investigation of the effect of Coriolis mixing reveals that the inclusion of rotational coupling terms in the Hamiltonian has negligible influence on the final branching results for detunings >30 cm^{-1}. Since most of the experimental data lies outside this detuning, we have chosen to ignore nonadiabatic Coriolis coupling in these calculations. This speeds up the numerical computation and eliminates an unessential complication in understanding the important physics. With this neglect of the rotational coupling terms, the 13-state problem reduces to a seven-state problem. In fact this reduction can be made more general. We may form linear combinations of the case (a) states corresponding to $\pm$ eigenstates of the reflection operator (through the collision plane). The out-of-plane Π orbital is then uncoupled from the in-plane orbitals in any case.[29] These linear combinations are analogous to the e/f parity eigenstates of Pouilly.[11] Based on the MSV potentials, $\Delta\sim-30$ cm^{-1} corresponds to an internuclear separation of $\sim9.5a_0$. This observation is consistent with a long-range orbital locking radius, $R_L\sim9.5a_0$, in reasonable agreement with previous estimates.[34]

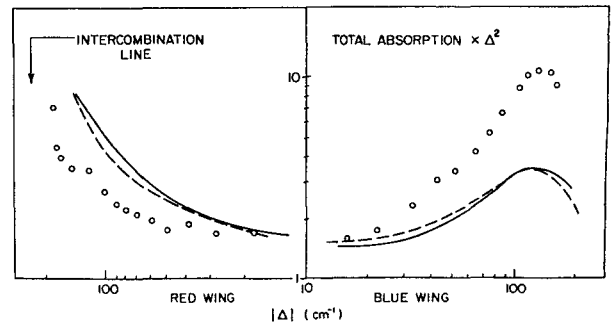

FIG. 3. Total absorption in the CaHe system as a function of detuning (Δ) from the Ca($4s^2\ ^1S-5p\ ^1P$) resonance line. The absorption profile has been multiplied by Δ^2. Open circles give data points. The curves are the theoretical model predictions: quantum close coupling (solid lines, from Ref. 11); classical trajectory close coupling (long dashed lines).

A. Total absorption profile

The experimentally observed far wing excitation profile is shown in Fig. 3, where we have graphed the total integrated fluorescence signal $[I(^1P)+I(^3P)]$ as a function of laser detuning $[(\omega-\omega_0)\equiv\Delta]$ from the Ca($4s^2\ ^1S_0-4s5p\ ^1P_1^0$) resonance. The profiles have been multiplied by Δ^2 in order to expand the scale and enhance the structure.

The profile in Fig. 3 indicates strong absorption in both red and blue wings. For larger detunings in the blue wing, we see evidence for a satellite near $\Delta\sim125$ cm^{-1}. Based on the model potential curves, this satellite is assigned to a maximum in the CaHe($4s^2\ ^1\Sigma^+-4s5p\ ^1\Sigma^+$) difference potential.

The red wing absorption shown in Fig. 3 is not as strong and also shows evidence of a rapid increase near $\Delta\sim175$ cm^{-1}. This structure corresponds to direct excitation of the Ca($4s^2\ ^1S-4s5p\ ^3P$) forbidden line at 273.5 nm. Indeed, it is not possible to separate entirely the excitation to the CaHe($4s5p\ ^1\Pi$) molecular state from excitation to the CaHe($4s5p\ ^3\Sigma^+$) state in the far red wing. It should also be noted that the CaHe($4s^2\ ^1\Sigma^+-4s5p\ ^1\Pi$) transition dipole moment function may show a marked variation in the region of the $^1\Sigma^+-^3\Sigma^+$ curve crossing.

The theoretical J-averaged result $I=\Sigma_J(2J+1)[N(^1P)+N(^3P)]$, represents the total absorption corresponding to the total excited state population, and is also shown in Fig. 3 (long dashed lines). The comparison with the experimental data is reasonably good and the blue wing satellite is reproducible in our calculations, although its strength is not well modeled. We also predict the steady red wing rise in absorption due to direct (nonadiabatic) $^3P_1$ state excitation. The solid lines represent the results from Pouilly's calculation of

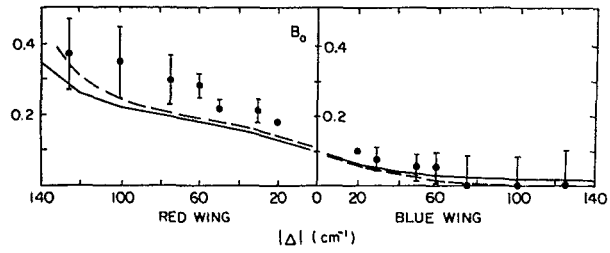

FIG. 4. Nascent branching fraction, $B_0=N(^3P)/[N(^1P)+N(^3P)]$, as a function of detuning (Δ) in the CaHe system. The curves give the result of theoretical modeling with the labels as in Fig. 3.

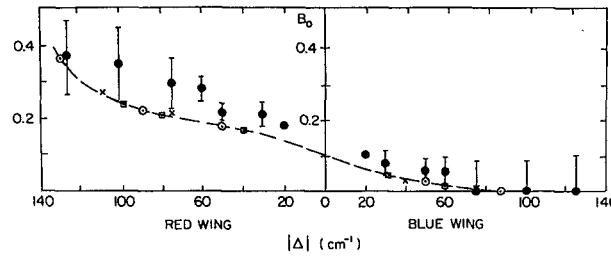

FIG. 5. Trajectory effects. Closed circles, experimental data; long dashed curve, algebraic average potential $\bar{V}=\frac{1}{13}\mathrm{Tr}(H)$; open circles, $V=0$; ×'s, ground state potential $\bar{V}=V(X\,^1\Sigma^+)$. The open squares show the results when rotational coupling is explicitly included.

the same quantity I, using the same model MSV potential curves.[11] While the essential qualitative features of the profiles in both wings are reproducible, both sets of calculated profiles deviate significantly from the experimentally measured profiles. This quantitative difference with experimental results must arise from inaccuracies in the model potential curves and/or to the neglect of the R dependence of the transition dipole moment function employed in the calculations.

B. Triplet branching ratio

We have measured the fluorescence ratio

$$\frac{I(^3P)}{I(^1P)+I(^3P)}$$

as a function of detuning (Δ) and He pressure. This data can be used to determine the *population* branching ratio

$$B=\frac{N(^3P)}{N(^1P)+N(^3P)} \tag{27}$$

by accounting for the weak fluorescence branching to states other than the $3d$ levels, and the relative spectral efficiency of the detection system.[9,10] At high pressures, where collisions mix the excited state populations on a time scale shorter than the radiative lifetimes, the branching ratio B approaches the thermal statistical limit independent of Δ. As the He pressure is decreased below ~2 Torr, the branching ratio B decreases rapidly and can be extrapolated to the zero pressure limit to obtain the nascent branching ratio, B_0.[9,10]

Figure 4 shows B_0 as a function of detuning, and clearly exhibits the expected red wing/blue wing asymmetry. The strong asymmetry in B_0 (approaching 100%) indicates a complete correlation between the $^1\Pi$ state excitation and the energy transfer process, in agreement with the curve-crossing model. It further demonstrates that absorption in the far wings ($\gtrsim$70 cm^{-1}) indeed occurs in a region where nonadiabatic $^1\Pi-^1\Sigma^+$ mixing can be neglected.

Figure 4 (long dashed lines) also shows the classical path calculation results obtained for the J-averaged branching ratio,

$$B_0=\frac{\Sigma_J(2J+1)N(^3P)}{\Sigma_J(2J+1)N(^1P)+\Sigma_J(2J+1)N(^3P)}.$$

The solid lines are the results obtained by Pouilly[11] and are included for comparison with our results. The rapid increase in the branching ratio in the far red wing is largely a result of direct excitation to the $^3\Sigma^+$ state and is correctly reproduced in our calculations. The good agreement obtained in our calculations with both experiment and with Pouilly's quantum mechanical results[11] demonstrates the validity of the semiclassical method for calculations of final state resolved nonadiabatic line shapes. This agreement further demonstrates the validity of the simplifying assumptions in our calculations, specifically, the neglect of rotational coupling and the use of angle-averaged radiative dipole coupling elements. The steady decrease in B_0 for blue wing detunings in the range Δ=20–70 cm^{-1} results from appreciable non-Franck–Condon or antistatic wing absorption; the assumption that red wing/blue wing excitation can be correlated entirely with $^1\Pi/^1\Sigma^+$ excitation becomes more exact as the detuning increases. It does *not* result from long-range Coriolis coupling in the entrance channel, which has been neglected in this calculation.

Thus, we conclude that the theoretical branching profiles are in extremely good agreement with the experimental data. The branching ratio depends on the dynamical coupling and is less sensitive to uncertainties in the shape of the potential energy curves.

C. Numerical tests

In order to ensure that we are indeed in the weak-field limit, we have varied the radiative coupling strength over two orders of magnitude from 0.58×10^{-2} cm^{-1} to 0.58 cm^{-1}, and we find no changes in the branching results.

The J averages were carried out from $J=0$ to $J=300$ in steps of five, to ensure convergence in the results at all detunings. Calculations carried out with a finer grid of J values gave virtually identical results. We have also included results in Fig. 5 when rotational coupling is included, for a few detunings (open squares), to illustrate its insignificance in determining B_0.

One of the primary features of our model is the use of a well-defined classical nuclear path. However, the concept of a well-defined trajectory is not rigorous. For the semiclassical approach to be valid, the final results should not be sensitive to this choice of trajectory. To verify this, we have carried out these calculations for different paths, i.e., for different potentials. The comparisons are given in Fig. 5. The

results discussed above have been obtained for $\bar{V}=\frac{1}{13}\mathrm{Tr}(H)$, a simple algebraic average potential (long dashed line in Fig. 5). Setting $\bar{V}=0$, leads to a straight line trajectory, with no repulsive inner wall (open circles). A choice of $\bar{V}=V(X\ ^1\Sigma^+)$ gives results for a trajectory determined by the ground state (×). This is essentially the population weighted average potential, since the total absorption is small. It is clear from Fig. 5 that these results are quite insensitive to the particular choice of classical path.

V. CONCLUSIONS

In summary, we have demonstrated the validity of a semiclassical (classical path quantum close coupling) method for modeling weak-field collisional redistribution including nonadiabatic spin–orbit and rotational-coupling effects. Analysis of the effect of rotational coupling on the branching ratio B_0, indicates that nonadiabatic rotational mixing ($^1\Pi-{}^1\Sigma^+$) in the entrance channel is negligible for detunings $\Delta\gtrsim 30\ \mathrm{cm}^{-1}$. This is consistent with an orbital locking radius of $\sim 9.5a_0$.

A significant computational simplification has been achieved here through the use of angle-averaged radiative-coupling matrix elements, which allows us to dispense with time-consuming numerical averages over collision geometries. The validity of this approximation for predicting total j-state populations in the weak-field limit is evidenced by good agreement with the full quantum results.

In a future publication we will apply this classical path method to model experimental results in the more complicated collisional energy transfer process[30]

$$\mathrm{Sr}^*(6p\ ^1P_1)+\mathrm{He}\rightarrow \mathrm{Sr}^*(6p\ ^3P_J)+\mathrm{He}$$

$$\rightarrow \mathrm{Sr}^*(5p4d\ ^3F_J)+\mathrm{He}$$

or

$$\mathrm{Sr}^*(6p\ ^1P_1)+\mathrm{He}\rightarrow \mathrm{Sr}^*(5p4d^1D_2)+\mathrm{He}.$$

In this case many additional channels are accessible. Quantum mechanical close-coupling calculations have not been attempted in this case. The excellent agreement we have demonstrated here suggests that the classical path method can be used with confidence.

ACKNOWLEDGMENTS

We gratefully acknowledge the support of the National Science Foundation for this work. We also thank B. Pouilly and W. C. Stwalley for helpful discussions and suggestions.

[1] M. O. Hale and S. R. Leone, J. Chem. Phys. **79**, 3352 (1983).
[2] M. O. Hale, I. V. Hertel, and S. R. Leone, Phys. Rev. Lett. **53**, 2296 (1984).
[3] W. Bussert and S. R. Leone, Chem. Phys. Lett. **138**, 269 (1988).
[4] W. Bussert, D. Neuschäfer, and S. R. Leone, J. Chem. Phys. **87**, 3833 (1987).
[5] A. Z. Devdariani and A. L. Zagrebin, Chem. Phys. Lett. **131**, 197 (1986).
[6] B. Pouilly and M. H. Alexander, J. Chem. Phys. **86**, 4790 (1987).
[7] M. H. Alexander and B. Pouilly, J. Chem. Phys. **90**, 5373 (1989); B. Pouilly, J. M. Robb, and M. H. Alexander, J. Chem. Phys. **91**, 1658 (1989).
[8] R. L. Dubs, P. S. Julienne, and F. H. Mies, J. Chem. Phys. **93**, 8784 (1990).
[9] K. C. Lin, P. D. Kleiber, J. X. Wang, W. C. Stwalley, and S. R. Leone, J. Chem. Phys. **89**, 4771 (1988).
[10] S. Ananthamurthy, P. D. Kleiber, W. C. Stwalley, and K. C. Lin, J. Chem. Phys. **90**, 7605 (1989).
[11] B. Pouilly, J. Chem. Phys. **95**, 5861 (1991).
[12] I. V. Hertel, Adv. Chem. Phys. **50**, 475 (1982).
[13] E. E. B. Campbell, H. Schmidt, and I. V. Hertel, Adv. Chem. Phys. **72**, 37 (1988).
[14] P. D. Kleiber, W. C. Stwalley, and K. M. Sando, Annu. Rev. Phys. Chem. **44**, 13 (1993).
[15] P. S. Julienne, Phys. Rev. A **26**, 3299 (1982).
[16] F. H. Mies, in *Theoretical Chemistry: Advances and Perspectives*, Vol. 6B, edited by D. Henderson (Academic, New York, 1981), p. 127.
[17] P. S. Julienne and F. H. Mies, Phys. Rev. A **30**, 831 (1984).
[18] P. S. Julienne and F. H. Mies, Phys. Rev. A **34**, 3792 (1986).
[19] L. L. Vahala, P. S. Julienne, and M. D. Harvey, Phys. Rev. A **34**, 1856 (1986).
[20] E. E. Nikitin, J. Chem. Phys. **43**, 744 (1965).
[21] F. Masnou-Seeuws and R. McCarroll, J. Phys. B **7**, 2230 (1974).
[22] J. B. Delos, Rev. Mod. Phys. **53**, 287 (1981).
[23] L. J. Kovalenko, S. R. Leone, and J. B. Delos, J. Chem. Phys. **91**, 6948 (1989).
[24] S. I. Yakovlenko, Sov. Phys. JETP **37**, 1019 (1973); V. S. Lisitsa and S. I. Yakovlenko, *ibid.* **39**, 759 (1974); V. S. Lisitsa and S. I. Yakovlenko, *ibid.* **41**, 233 (1975).
[25] N. M. Kroll and K. M. Watson, Phys. Rev. A **8**, 804 (1973); **13**, 1018 (1976).
[26] P. L. DeVries and T. F. George, Mol. Phys. **36**, 151 (1978); K. S. Lam and T. F. George, J. Chem. Phys. **76**, 3396 (1982).
[27] J. C. Light and A. Szöke, Phys. Rev. A **18**, 1363 (1978).
[28] P. D. Kleiber, J. Cooper, K. Burnett, C. V. Kunasz, and M. G. Raymer, Phys. Rev. A **27**, 291 (1983).
[29] R. J. Bieniek, P. S. Julienne, and F. Rebentrost, J. Phys. B **24**, 5103 (1991).
[30] S. Ananthamurthy, P. D. Kleiber, and K. M. Sando (unpublished).
[31] J. T. Hougen, NBS Monograph 115 (1970).
[32] P. L. DeVries and T. F. George, Phys. Rev. A **18**, 1751 (1978).
[33] F. H. Mies, P. S. Julienne, P. S. Band, and S. J. Singer, J. Phys. B **19**, 3249 (1986).
[34] B. Pouilly and M. H. Alexander, Chem. Phys. **145**, 191 (1990).